frontiers | Frontiers in Earth Science

ORIGINAL RESEARCH
published: 30 May 2022
doi: 10.3389/feart.2022.911147

# Origin and Trace of Hydrothermal Calcites in the Hydrocarbon Reservoirs Intruded by Diabase: Evidence From Strontium and Oxygen Isotopic Proxies

*Chao Liu[1,2,3]*, Rui Xue[4], Zhiwei Jia[5], Xiaodong Zhao[4], Ke Wang[1,3], Yong Yang[6], Junhao He[1,3], Ping Liu[7] and Zhigang Liu[7]*

[1]College of Geosciences and Engineering, Xi'an Shiyou University, Xi'an, China, [2]State Key Laboratory of Petroleum Resources and Prospecting, China University of Petroleum, Beijing, China, [3]Shaanxi Key Lab of Petroleum Accumulation Geology, Xi'an Shiyou University, Xi'an, China, [4]Twelfth Oil Production Plant, Changqing Oil Field Company of PetroChina, Heshui, China, [5]Research Institute of Drilling & Production Technology of Qinghai Oilfield Company, Dunhuang, China, [6]Hubei Geological Bureau, Wuhan, China, [7]Oil Production Plant of Huabei Oilfield Company, PetroChina, Xinji, China

OPEN ACCESS

**Edited by:**
Chen Zhang,
Chengdu University of Technology, China

**Reviewed by:**
Qingbin Xie,
China University of Petroleum, Beijing, China
Yannick Tepinhi,
Schlumberger, United States
Guiwen Wang,
China University of Petroleum, Beijing, China

***Correspondence:**
Chao Liu
liuchao_xsyu@163.com

**Specialty section:**
This article was submitted to Structural Geology and Tectonics, a section of the journal Frontiers in Earth Science

**Received:** 02 April 2022
**Accepted:** 14 April 2022
**Published:** 30 May 2022

**Citation:**
Liu C, Xue R, Jia Z, Zhao X, Wang K, Yang Y, He J, Liu P and Liu Z (2022) Origin and Trace of Hydrothermal Calcites in the Hydrocarbon Reservoirs Intruded by Diabase: Evidence From Strontium and Oxygen Isotopic Proxies. Front. Earth Sci. 10:911147. doi: 10.3389/feart.2022.911147

Thermal contact clastic rocks provide a new potential type of hydrocarbon reservoirs for expanding exploration targets. However, the development mechanism of this type of reservoir remains enigmatic. Authigenic hydrothermal carbonates associated with magmatism exert significant controls over physical properties of the contact reservoirs. Therefore, the origin and trace of hydrothermal carbonates are key issues for reservoir development elucidation of thermal contact reservoirs and need to be further investigated. The current study takes the typical hydrocarbon area of thermal contact metasandstone reservoirs from the Funing Formation, northern Slope of Gaoyou sag, as a case study, aiming to unravel the origin and trace of authigenic hydrothermal calcites developed in thermal contact reservoirs, mainly using strontium and oxygen isotopic geochemistry proxies combined with petrological and mineralogical analyses. Authigenic hydrothermal calcites are distinguished, and their distribution characteristics are examined in thermal contact rocks. Subsequently, the origin and migration trace of the hydrothermal-related calcites are clarified. This study has significant implications for intensive understanding of reservoir development mechanism and reservoir evaluation and prediction of thermal contact clastic rocks.

**Keywords: thermal contact rocks, hydrothermal calcites, contact diagenesis, Gaoyou sag, Funing Formation**

## INTRODUCTION

In recent decades, numerous hydrocarbon reservoirs at the contact zones of magmatic intrusions were continuously explored in many sedimentary basins worldwide. Furthermore, the contact metamorphic zone and intrusive edge can act as an integrated reservoir (Zhang, 2000; Wu et al., 2006; Liu et al., 2019). This finding has challenged the conventional perspective, which concluded that hydrocarbon should not occur at the vicinity to magmatic zone. In eastern China, massive thermal contact metamorphic reservoirs were explored in the Mesozoic–Cenozoic rifted basins, which were characterized by wide occurrence of frequent and wide-range magmatic activities. In

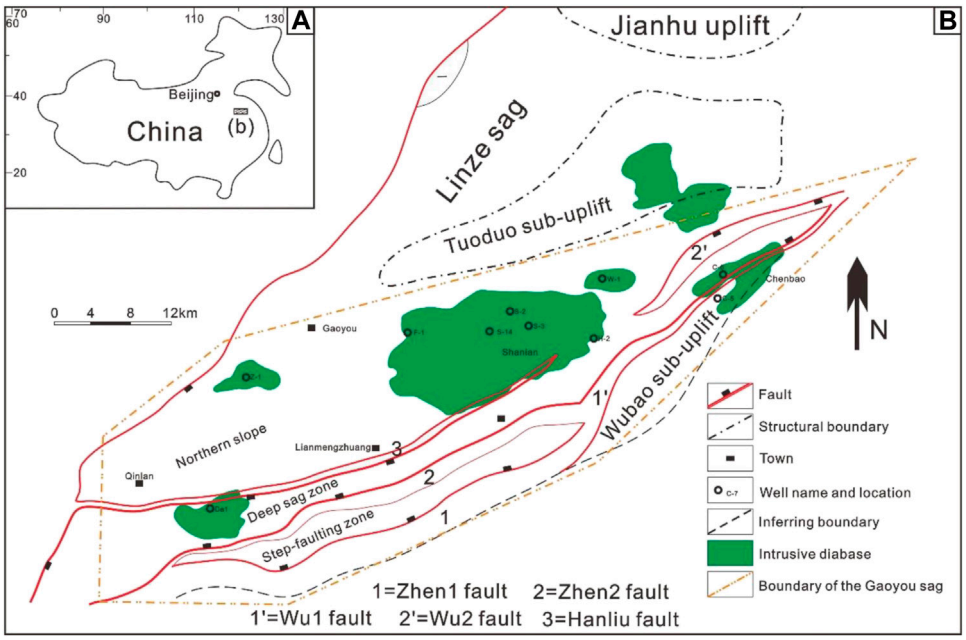


**FIGURE 1 | (A)** General location of the Gaoyou sag. **(B)** Structural map showing the distribution of intrusive diabase and well locations at the studied interval (modified after Liu et al., 2019).

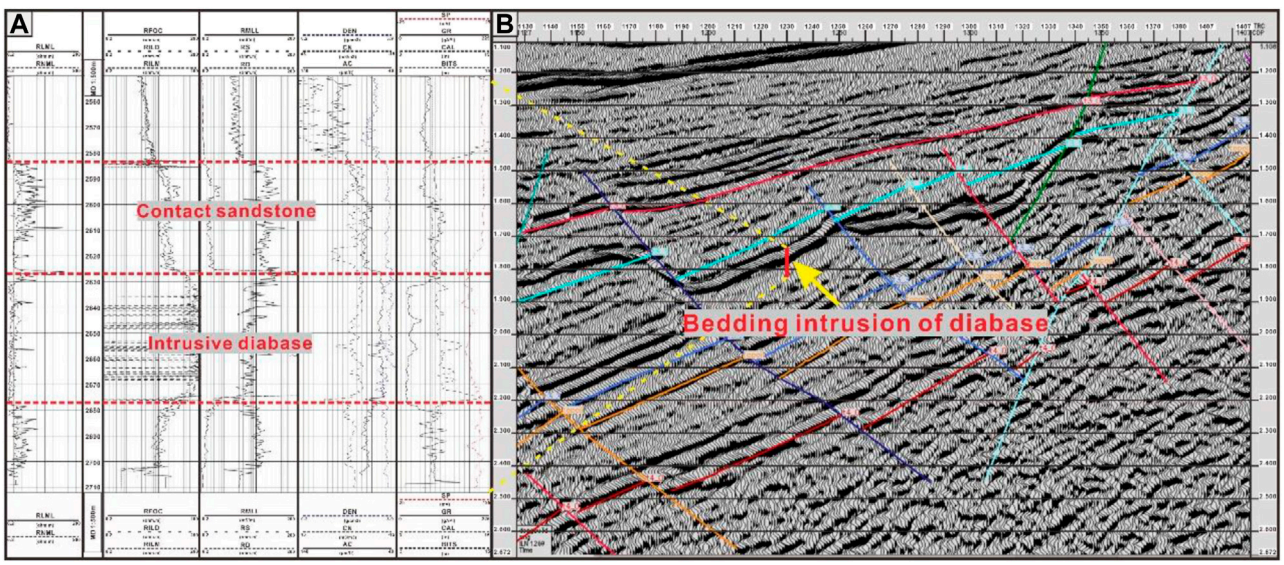


**FIGURE 2 |** Well-logging data **(A)** and seismic profile **(B)** showing spatial distribution of intrusive diabase and contact sandstones in the Gaoyou sag.

particular, mudstones can be altered to be potential hydrocarbon reservoirs after the thermal contact metamorphism caused by magmatic intrusion. For instance, metamudstone reservoirs in the Dongying sag and slate reservoirs in the Jizhong sag are becoming critical hydrocarbon reserves in the Bohai Bay basin (e.g., Wu et al. and Liu et al., 2016).

Previous studies have documented that multiple authigenic minerals (e.g., carbonates, quartz, and clay-related metamorphic minerals) were formed in contact zones of intrusive magma during contact diagenesis (Ros, 1998). These authigenic minerals have influences on reservoir petrophysics at different degrees, thus being important subject for developing mechanism of hydrocarbon reservoirs (Rateau et al., 2013; Liu et al., 2016). In particular, the authigenic carbonate had critical controls on reservoir because it was very sensitive to fluid environment (i.e., it could precipitate or be dissolved in fluids of different

**TABLE 1 |** Petrophysical features measured from the cored wells (note that 1) Por-c refers to porosity values obtained by using the point counting method in the current study; 2) Por-m refers to porosity values obtained by laboratory measurements; and 3) Por-m and permeability are provided by report from the Jiangsu Oilfield).

| Well | Depth (m) | Lithology | Por-c (%) | Por-m (%) | Permeability (mD) |
|---|---|---|---|---|---|
| S-2 | 1898.05 | Graywacke | 18.35 | 14.89 | 22.69 |
| S-2 | 1908.55 | Graywacke | 17.52 | 16.88 | 33.56 |
| S-2 | 1909.48 | Graywacke | 20.36 | 22.21 | 45.89 |
| S-2 | 1913.58 | Metasandstone | 15.21 | 15.69 | 29.87 |
| S-2 | 1918.61 | Metasandstone | 14.31 | 16.89 | 15.69 |
| S-2 | 1921.33 | Metasandstone | 17.01 | 16.55 | 31.58 |
| S-2 | 1928.88 | Metasandstone | 19.86 | 14.58 | 89.56 |
| S-2 | 1937.98 | Metasandstone | 21.25 | 20.01 | 56.81 |
| S-2 | 1945.69 | Metasandstone | 11.36 | 15.36 | 44.51 |
| S-2 | 1951.09 | Metasandstone | 28.65 | 24.15 | 76.01 |
| S-2 | 1963.25 | Metasandstone | 22.71 | 20.08 | 59.81 |
| S-2 | 1975.33 | Metasandstone | 20.05 | 17.87 | 45.55 |
| S-2 | 1980.12 | Metasandstone | 17.20 | 15.89 | 40.89 |
| S-2 | 1988.56 | Metasandstone | 16.45 | 18.21 | 38.86 |
| S-2 | 1998.33 | Metasandstone | 15.23 | 16.33 | 65.23 |
| S-2 | 2000.55 | Diabase | 10.89 | 11.55 | 21.89 |
| S-2 | 2003.69 | Diabase | 8.98 | 4.59 | 10.55 |
| S-2 | 2008.01 | Diabase | 7.50 | 6.11 | 16.87 |
| S-14 | 1848.53 | Quartzwacke | 30.59 | 28.97 | 105.88 |
| S-14 | 1853.57 | Quartzwacke | 31.55 | 31.58 | 118.47 |
| S-14 | 1859.13 | Quartzwacke | 32.80 | 31.13 | 251.12 |
| S-14 | 1863.88 | Metasandstone | 21.89 | 22.91 | 201.48 |
| S-14 | 1869.12 | Metasandstone | 22.20 | 21.56 | 155.29 |
| S-14 | 1875.93 | Metasandstone | 29.41 | 27.46 | 178.56 |
| S-14 | 1883.69 | Metasandstone | 30.52 | 28.41 | 298.81 |
| S-14 | 1890.55 | Metasandstone | 19.48 | 17.54 | 178.33 |
| S-14 | 1896.78 | Metasandstone | 26.65 | 23.68 | 121.55 |
| S-14 | 1902.12 | Metasandstone | 24.89 | 21.12 | 90.87 |
| S-14 | 1908.15 | Metasandstone | 21.89 | 21.58 | 133.56 |
| S-14 | 1921.58 | Metasandstone | 19.51 | 19.99 | 68.87 |
| S-14 | 1929.56 | Metasandstone | 18.45 | 18.56 | 65.55 |
| S-14 | 1937.12 | Metasandstone | 17.51 | 17.07 | 50.81 |
| S-14 | 1948.01 | Metasandstone | 15.55 | 15.78 | 55.61 |
| S-14 | 1955.56 | Metasandstone | 13.78 | 12.15 | 40.71 |
| S-14 | 1960.52 | Metasandstone | 19.78 | 16.89 | 98.98 |
| S-14 | 1968.13 | Diabase | 5.23 | 4.33 | 10.88 |
| S-14 | 1971.12 | Diabase | 9.84 | 9.05 | 15.59 |
| S-14 | 1973.25 | Diabase | 6.65 | 6.78 | 19.87 |
| S-3 | 1998.55 | Graywacke | 20.02 | 23.38 | 113.99 |
| S-3 | 2003.18 | Graywacke | 21.35 | 21.37 | 165.81 |
| S-3 | 2007.91 | Graywacke | 26.60 | 25.50 | 187.71 |
| S-3 | 2013.15 | Metasandstone | 22.56 | 22.89 | 185.56 |
| S-3 | 2018.66 | Metasandstone | 17.78 | 17.07 | 97.78 |
| S-3 | 2024.91 | Metasandstone | 16.58 | 14.21 | 85.65 |
| S-3 | 2028.05 | Metasandstone | 16.21 | 13.89 | 81.13 |
| S-3 | 2031.38 | Metasandstone | 15.23 | 12.08 | 50.28 |
| S-3 | 2035.63 | Metasandstone | 20.09 | 15.87 | 45.87 |
| S-3 | 2039.14 | Metasandstone | 21.13 | 17.89 | 33.85 |
| S-3 | 2043.14 | Metasandstone | 22.58 | 20.87 | 185.45 |
| S-3 | 2049.63 | Metasandstone | 18.78 | 18.88 | 167.25 |
| S-3 | 2058.11 | Metasandstone | 16.58 | 16.41 | 80.56 |
| S-3 | 2067.95 | Metasandstone | 18.68 | 17.56 | 115.48 |
| S-3 | 2076.15 | Metasandstone | 19.87 | 19.09 | 178.14 |
| S-3 | 2086.53 | Diabase | 4.23 | 4.58 | 15.51 |
| S-3 | 2089.98 | Diabase | 4.98 | 4.71 | 10.24 |
| S-3 | 2092.36 | Diabase | 3.87 | 4.39 | 9.89 |

temperatures or metal concentrations; Therkelsen, 2016; Liu et al., 2019). However, the origin and migration pathways are still enigmatic due to chemical property instability and complicated fluid environment of hydrothermal carbonates, which confined our further understanding of developing mechanism of the contact metamorphic reservoirs.

Taking the Funing Formation of Gaoyou sag, Subei Basin, as a case study in the current research, we mainly adopted

**TABLE 2 |** Strontium and oxygen isotopes measured from cored wells in the studied area.

| Well | Depth (m) | Lithology | Mineralogy | $^{87}Sr/^{86}Sr$ | $\delta^{18}O$ (‰) |
|---|---|---|---|---|---|
| S-2 | 1898.05 | Graywacke | Coarse-sized calcite | 0.708248 | 26.11 |
| S-2 | 1908.55 | Graywacke | Coarse-sized calcite | 0.708295 | 26.28 |
| S-2 | 1909.48 | Graywacke | Coarse-sized calcite | 0.708251 | 27.53 |
| S-2 | 1913.58 | Metasandstone | Fine-sized calcite | 0.707398 | 17.33 |
| S-2 | 1918.61 | Metasandstone | Fine-sized calcite | 0.707381 | 16.58 |
| S-2 | 1921.33 | Metasandstone | Fine-sized calcite | 0.707425 | 20.11 |
| S-2 | 1928.88 | Metasandstone | Fine-sized calcite | 0.707351 | 15.11 |
| S-2 | 1937.98 | Metasandstone | Fine-sized calcite | 0.707398 | 13.68 |
| S-2 | 1945.69 | Metasandstone | Fine-sized calcite | 0.707425 | 13.77 |
| S-2 | 1951.09 | Metasandstone | Fine-sized calcite | 0.707388 | 13.05 |
| S-2 | 1963.25 | Metasandstone | Fine-sized calcite | 0.707321 | 12.89 |
| S-2 | 1975.33 | Metasandstone | Fine-sized calcite | 0.707115 | 12.31 |
| S-2 | 1980.12 | Metasandstone | Fine-sized calcite | 0.707101 | 12.85 |
| S-2 | 1988.56 | Metasandstone | Fine-sized calcite | 0.707056 | 12.03 |
| S-2 | 1998.33 | Metasandstone | Fine-sized calcite | 0.707003 | 11.25 |
| S-2 | 2000.55 | Diabase | Fine-sized calcite | 0.706999 | 10.25 |
| S-2 | 2003.69 | Diabase | Fine-sized calcite | 0.706815 | 9.88 |
| S-2 | 2008.01 | Diabase | Fine-sized calcite | 0.706825 | 9.41 |
| S-14 | 1848.53 | Quartzwacke | Coarse-sized calcite | 0.708226 | 27.35 |
| S-14 | 1853.57 | Quartzwacke | Coarse-sized calcite | 0.708214 | 27.15 |
| S-14 | 1859.13 | Quartzwacke | Coarse-sized calcite | 0.708336 | 26.55 |
| S-14 | 1863.88 | Metasandstone | Coarse-sized calcite | 0.707601 | 16.75 |
| S-14 | 1869.12 | Metasandstone | Coarse-sized calcite | 0.707611 | 16.52 |
| S-14 | 1875.93 | Metasandstone | Coarse-sized calcite | 0.707628 | 16.23 |
| S-14 | 1883.69 | Metasandstone | Coarse-sized calcite | 0.707633 | 15.12 |
| S-14 | 1890.55 | Metasandstone | Coarse-sized calcite | 0.707551 | 15.36 |
| S-14 | 1896.78 | Metasandstone | Coarse-sized calcite | 0.707523 | 12.58 |
| S-14 | 1902.12 | Metasandstone | Coarse-sized calcite | 0.707503 | 12.44 |
| S-14 | 1908.15 | Metasandstone | Coarse-sized calcite | 0.707486 | 11.05 |
| S-14 | 1921.58 | Metasandstone | Coarse-sized calcite | 0.707489 | 11.18 |
| S-14 | 1929.56 | Metasandstone | Coarse-sized calcite | 0.707423 | 11.86 |
| S-14 | 1937.12 | Metasandstone | Coarse-sized calcite | 0.707412 | 10.59 |
| S-14 | 1948.01 | Metasandstone | Coarse-sized calcite | 0.707211 | 10.48 |
| S-14 | 1955.56 | Metasandstone | Coarse-sized calcite | 0.707005 | 10.56 |
| S-14 | 1960.52 | Metasandstone | Coarse-sized calcite | 0.706991 | 9.98 |
| S-14 | 1968.13 | Diabase | Coarse-sized calcite | 0.706511 | 9.62 |
| S-14 | 1971.12 | Diabase | Coarse-sized calcite | 0.706198 | 9.12 |
| S-14 | 1973.25 | Diabase | Coarse-sized calcite | 0.706221 | 9.05 |
| S-3 | 1998.55 | Graywacke | Coarse-sized calcite | 0.708489 | 26.78 |
| S-3 | 2003.18 | Graywacke | Coarse-sized calcite | 0.708441 | 25.98 |
| S-3 | 2007.91 | Graywacke | Coarse-sized calcite | 0.708135 | 26.88 |
| S-3 | 2013.15 | Metasandstone | Fine-sized calcite | 0.707915 | 17.68 |
| S-3 | 2018.66 | Metasandstone | Fine-sized calcite | 0.707936 | 18.88 |
| S-3 | 2024.91 | Metasandstone | Fine-sized calcite | 0.707715 | 18.01 |
| S-3 | 2028.05 | Metasandstone | Fine-sized calcite | 0.707688 | 14.58 |
| S-3 | 2031.38 | Metasandstone | Fine-sized calcite | 0.707605 | 14.99 |
| S-3 | 2035.63 | Metasandstone | Fine-sized calcite | 0.707618 | 14.31 |
| S-3 | 2039.14 | Metasandstone | Fine-sized calcite | 0.707521 | 13.78 |
| S-3 | 2043.14 | Metasandstone | Fine-sized calcite | 0.707158 | 12.89 |
| S-3 | 2049.63 | Metasandstone | Fine-sized calcite | 0.707225 | 13.11 |
| S-3 | 2058.11 | Metasandstone | Fine-sized calcite | 0.707008 | 13.01 |
| S-3 | 2067.95 | Metasandstone | Fine-sized calcite | 0.707105 | 10.89 |
| S-3 | 2076.15 | Metasandstone | Fine-sized calcite | 0.707002 | 9.26 |
| S-3 | 2086.53 | Diabase | Fine-sized calcite | 0.706158 | 9.05 |
| S-3 | 2089.98 | Diabase | Fine-sized calcite | 0.706568 | 9.11 |
| S-3 | 2092.36 | Diabase | Fine-sized calcite | 0.706112 | 9.36 |

strontium and oxygen isotopic analysis, coupled with petrophysical measurement and lithology and mineralogy study, to elucidate and decipher the origin and trace of hydrothermal carbonates in the hydrocarbon reservoir intruded by diabase. This study provides mechanism understanding for reservoir diagenesis associated to magmatic intrusion, thus having great significance for reservoir assessment and prediction.

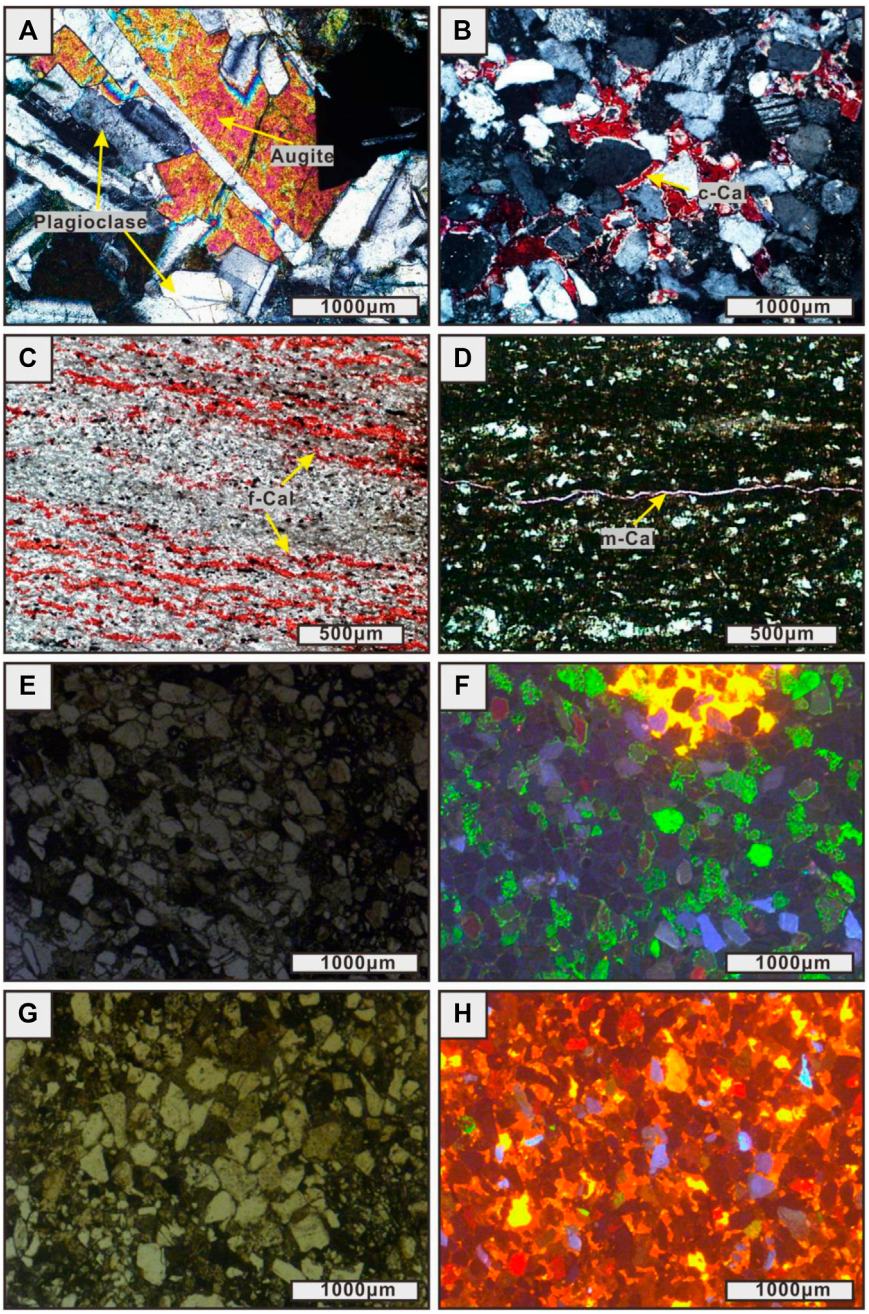


**FIGURE 3 |** Photomicrographs showing the lithology of intrusive and contact metamorphic zone from the studied interval. **(A)** Columnar plagioclase grains are randomly distributed with frame spaces being filled with augite grains, composing typical diabasic texture. Z-1 well, 1,615.55 m, cross-polarized light (XPL). **(B)** Coarse-sized calcites (c-Cal) are developed as cements of quartz or feldspar grains in the contact sandstones, coated by dolomite rinds. C-6 well, 2011.68 m, XPL. **(C)** Fine-sized calcites (f-Cal) are linearly distributed along micropores developed in the contact sandstones. S-7 well, 2,683.88 m, plane-polarized light (PPL). **(D)** Micritic calcites (m-Cal) are developed in fractures in contact sandstones. C-6 well, 2015.44 m, XPL. **(E)** f-Cal-type dominated sandstones (PPL) commonly show **(F)** blue to purple cathodoluminescence feature (CL). S-7 well, 2,866.15 m. **(G)** c-Cal-type dominated sandstones (PPL) usually display **(H)** orange to red CL characteristics. C-6 well, 2035.18 m.

## GEOLOGICAL SETTING

The Subei Basin, located in eastern China (**Figure 1A**), is a rifted basin developed from the Mesozoic and Paleozoic basement. The Subei Basin comprises the Dongtai and Yanfu depressions and the Jianhu uplift, covering a total area of ~ $3.5\,km^2 \times 10^4\,km^2$. The Gaoyou sag was formed at the center of the Dongtai depression due to uneven uplifting caused by late Cretaceous Yizheng movement

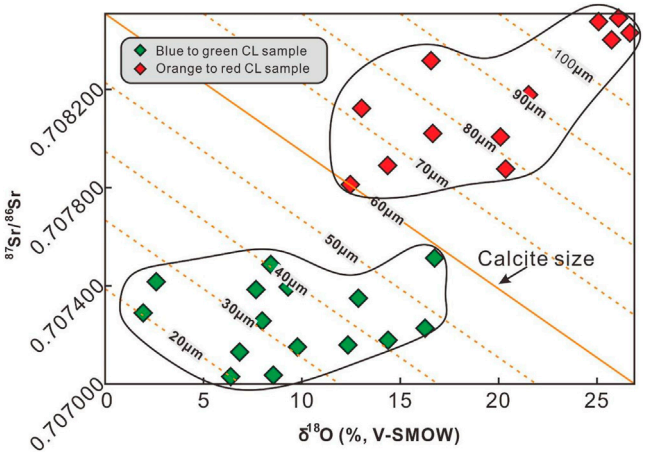


**FIGURE 4 |** Integrated scatter diagram showing calcite sample clustering of different sizes, CL, and strontium and oxygen isotopes. Detailed description is given in the text.

and Cenozoic Wubao movement (Yang and Chen, 2003; Liu et al., 2016). The northern slope, covering an area of 1,300 $km^2$, is a major hydrocarbon zone of the Gaoyou sag (**Figure 1B**).

Diabase dikes and sills are widely distributed in the Gaoyou sag, particularly in the northern slope (**Figure 1B**). Previous studies revealed that two stages of magmatic activities occurring during the period of Sanduo movement were related to diabase intrusion in the Funing Formation of the Gaoyou sag (Mao, 2000; Hu, 2010). Well-logging and seismic interpretations reveal that diabase intruded dominantly as hypabyssal or concordant sills and multiphase intrusive diabase were superimposed complexes with thicknesses ranging from several meters to more than 200 m (Wang et al., 2007; **Figures 2A,B**). The diabases and contacting metamorphic zones (metamudstones and metasandstones), characterized by low porosity and permeability and high heterogeneity, are important hydrocarbon reserves in the northern slope of the Gaoyou sag. Thus far, nearly eighty production wells have been drilled, and commercial oil and gas flow have been found in 20 wells in the Matouzhuang, Huazhuang, Facaizhaunge, Xiejiazhuang, Shanian, and Chenbao regions (**Figure 1**). To date, 2.4 t × $10^4$ t of crude oil has been produced in diabase and their contact metamorphic complex reservoirs (Liu et al., 2019).

## SAMPLES AND METHODS

Core samples with a total length of 82.50 m were obtained from exploration wells (see **Figure 1**). Full-length core specimens were analyzed preliminarily at fieldwork to avoid weathering surfaces or veins for further experimental measurements.

Multiple microscopic observations were conducted on impregnated, casting, and CL thin sections. The detailed observation procedures are referred to Liu et al. (2016). The mineral contents and porosities were determined by image analysis, using the point counting method (i.e., counting 300 points on a single piece of thin sections). The result is given in the **Table 1**.

Strontium and oxygen isotopes ($^{87}Sr/^{86}Sr$ and $\delta^{18}O$) were analyzed using micro-area and *in situ* methods by applying the laser ablation method. The marked thin sections were sent for LA-ICP-MS (an LSX-200 UV laser ablation system equipped with an NdYAG laser emitter and a helium carrier). Detailed parameter settings were carried out following Liu et al. (2017). The detection error was better than ±0.000002 and ±0.1‰ for $^{87}Sr/^{86}Sr$ and $\delta^{18}O$, respectively. All $\delta^{18}O$ data were documented as V-SMOW standard. All the measured isotopic data are given in **Table 2**.

The analyses mentioned previously were exclusively conducted at the State Key Laboratory of Petroleum Resources and Prospecting in China University of Petroleum, Beijing.

## RESULTS

### Lithology and Mineralogy

The intrusive rock is mainly composed of basic plagioclase and augite of ~ 50 and ~ 40%, respectively. It displays a typical diabasic texture which is characterized by similar grain sizes of plagioclase and augite grains and the frame spaces of plagioclase grains filled with augite, chlorite, and hematite grains (**Figure 3A**). Some other minor minerals, including olivine, biotite, and apatite, are developed. Chloritization widely occurs at the diabase edges. In the closely contacting metasandstones, three types of authigenic carbonates can be classified according to morphologies, sizes, and cathodoluminescences: 1) coarse-sized calcites—they are usually developed as pore-filling cements among quartz grains characterized by coarse sizes ranging from 200 to 500 μM; for example, dolomite coating is commonly developed as rinds in the contact metasandstones (**Figure 3B**); 2) fine-sized calcites—this type of calcites, with sizes ranging from 50 to 200 μM, commonly occur as authigenic mineral fillings in micropores of the metasandstones and are often distributed in array (**Figure 3C**); and 3) micritic calcites—this type of calcites is characterized by sizes usually less than 50 μM and distributed in fractures or microfissures of the contact metasandstones (**Figure 3D**). The fine-sized and micritic calcites often display blue to purple CL features (**Figures 3E,F**). On the contrary, the coarse-sized calcites usually exhibit orange to red CL features (**Figures 3G,H**).

### Strontium and Oxygen Isotopes

*Strontium isotope* ($^{87}Sr/^{86}Sr$): Strontium isotopes from three different zones, namely, the diabase intrusion, the contact metasandstones, and the overlying unaltered sandstones (**Figure 2**), showed significant variations. The $^{87}Sr/^{86}Sr$ ratios of the unaltered sandstones ranged from 0.708135 to 0.708489, with a mean value of 0.708293. On the contrary, the altered metasandstones influenced by diabase intrusion exhibited low $^{87}Sr/^{86}Sr$ ratios, with the values ranging from 0.706991 to 0.707936 and the mean value of 0.707393. The diabase edge exhibited extremely low $^{87}Sr/^{86}Sr$ values compared with metasandstones, with $^{87}Sr/^{86}Sr$ ratios ranging from 0.706112 to 0.707000 and a mean value of 0.706490 (**Table 2**).

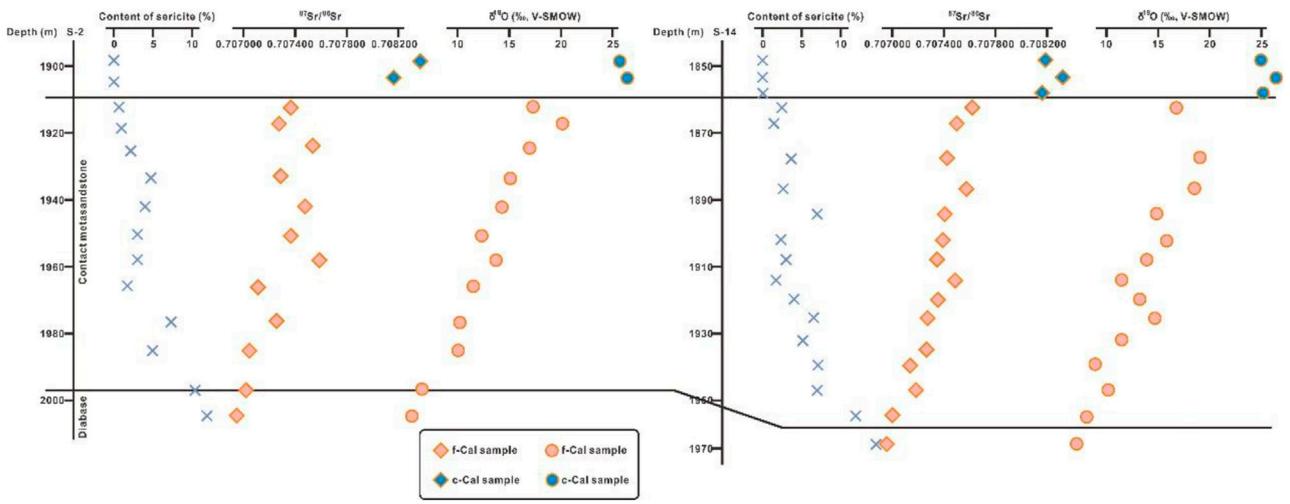


**FIGURE 5 |** Lithology-based correlation of wells S-2 and S-14 showing the evolution of strontium and oxygen isotopes and sericite contents. Detailed interpretation is provided in the text.

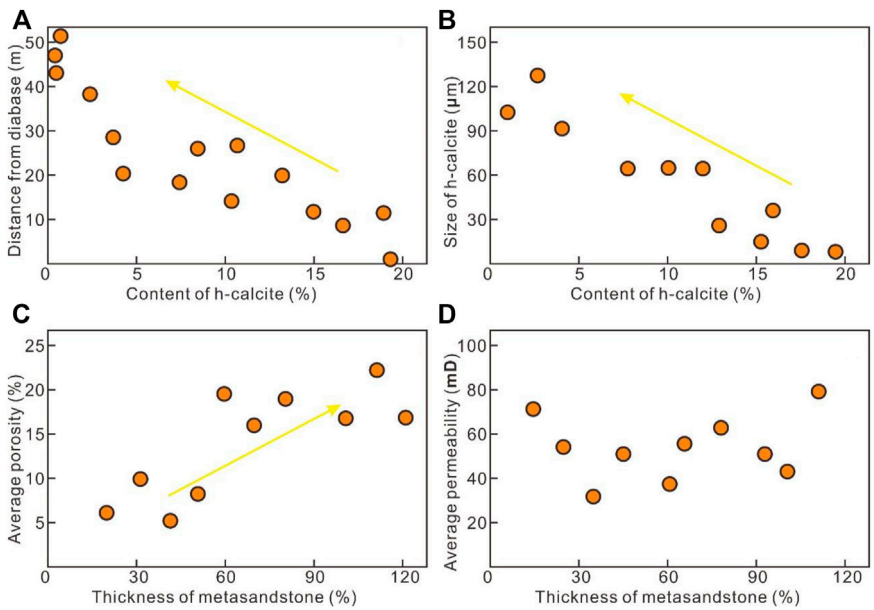


**FIGURE 6 |** Crossplots **(A)** and **(B)** showing the correlations of the content of hydrothermal-origin calcites (h-calcite) *versus* distance from diabase and hydrothermal-origin calcite size, respectively. Crossplots **(C)** and **(D)** showing the correlations of thickness of metasandstone *versus* average porosity and permeability of contact metasandstones, respectively. Detailed explanation is given in the text.

*Oxygen isotope* ($\delta^{18}O$): Similar to strontium isotopes, oxygen isotopes from the three different zones exhibited pronouncedly variable ratios, with their values ranging from 25.98 to 27.53‰ (mean value of 26.73‰), from 9.26 to 20.11‰ (mean value of 13.76‰), and from 9.05 to 10.25‰ (mean value of 9.43‰) of unaltered sandstones, contact metasandstones, and intrusive diabase, respectively (**Table 2**).

## Porosity and Permeability

The porosities from the point counting method and experimental measurement exhibited similar values of unaltered sandstones, contact metasandstones, and intrusive diabase, with their values ranging from 14.89 to 32.80% (mean value of 24.17%), from 11.36 to 30.52% (mean value of 19.08%), and from 3.87 to 11.55% (mean value of 6.57%), respectively (**Table 1**). The permeability of the three zones, namely, the overlying unaltered sandstones,

the contact metasandstones, and the diabase intrusion, exhibited different ratios, with values ranging from 22.69 mD to 251.12 mD (mean value of 116.12 mD), from 15.69 mD to 298.81 (mean value of 95.80 mD), and from 9.89 mD to 21.89 mD (mean value of 14.59 mD), respectively (**Table 1**).

# DISCUSSION

## Calcite Origins

Except for autochthonous calcites being precipitated during the syndepositional period, the allochthonous carbonates formed at the diagenetic stage is another major source of calcite. The latter source of carbonates fills reservoir pores as authigenic minerals, thus controlling the reservoir property significantly (Huang, 1990; Vahrenkamp and Swart, 1990; Machel and Burton, 1994; Warren, 2000; Machel, 2004; Liu et al., 2022). In the studied interval, the calcite samples are accumulated into two clusters according to their mineral sizes, morphologies, CL lights, and strontium and oxygen isotopes (**Figure 4**). The strontium isotope composition ($^{87}Sr/^{86}Sr$) of the diagenetic carbonates is mainly composed of two contrasting sources, namely, high radiogenic "continental Sr" derived from terrestrial flow and low radiogenic "mantle Sr" of magmatic origin with values of 0.712 ± 0.001 and 0.703000, respectively (McArthur et al., 2001; Korte et al., 2003; Huang et al., 2008). The variation of two sources determined the $^{87}Sr/^{86}Sr$ composition of authigenic carbonates. Obviously, the studied fine-/micritic-sized calcites should originate from the hydrothermal components produced by diabase intrusion because the $^{87}Sr/^{86}Sr$ composition of these calcite samples is close to mantle Sr. This inference is consistent with other features. First, the temperature of the hydrothermal fluids introduced by magmatism was often much higher than that of diagenetic fluids, thus displaying pronouncedly depleted oxygen isotopes (**Figure 5**). Second, cathodoluminescences are different in calcites of different origins, with terrestrial-origin calcite displaying orange to red color CL, marine-origin calcite exhibiting no CL feature, and magmatic-origin calcite showing blue to purple CL light (Huang, 1990; Veizer et al., 1999). The CL feature of the studied fine-/micritic-sized calcites indicated their magmatic source. Moreover, the temperature decreases rapidly when hydrothermal fluids intrude into contact sandstones, thus resulting in rapid crystallization of authigenic minerals and forming fine-sized calcites (Heald and Rention, 1966; Robert et al., 2005; Liu et al., 2015). On the contrary, the calcites characterized by orange to red CL lights exhibit typical terrestrial-origin features with respect to coarse mineral sizes and high $^{87}Sr/^{86}Sr$ ratios. Hence, the fine- and micritic-sized calcites originated from hydrothermal fluids are related to diabase intrusion in the studied area, while the coarse-sized calcite cements were derived from diagenetic fluids occurring before this magmatism.

## Trace of Hydrothermal Calcites

High-temperature magma can heat formation water, thus driving water convection in connected porosities of the reservoir sandstones when diabase is intruding into overlying formation (Enrique et al., 1997; Liu et al., 2015). It is believed that hydrothermal fluids circulate for many times and water–rock reactions repeatedly occur in the rock frame until the temperature difference disappears between the hydrothermal fluids and formation water (Etheridge et al., 1983; Wood and Walther, 1986). However, the hydrothermal convection may not occur under a complex situation, especially when the rock framework collapsed to maintain pressure balance and the porosity system was not connected (Haszeldine et al., 1984; Knut et al., 1988). In this scenario, upward unidirectional flow occurs (Wood and Walther). In the studied interval of the Gaoyou sag, strontium and oxygen isotopes increased constantly at an upward direction (**Figure 5**), revealing that the proportion of hydrothermal fluid was constantly decreasing. Hence, unidirectional flow, instead of the hydrothermal convection, occurred during the intrusion of diabase in the studied area. Otherwise, it should exhibit homogeneous isotopic features due to multiple circulation of flows. This inference is consistent with the fact that contents of hydrothermal calcites decreased constantly (**Figures 6A,B**). It is noteworthy that the range of metasandstone influenced by diabase intrusion is closely associated with porosity but is weakly linked with permeability (**Figures 6C,D**). This correlation in the studied interval reveals that the intrusion of diabase brought massive energy, thereby causing indiscriminate breakthrough of hydrothermal fluids in the contact sandstones. However, large pores could accommodate more high-energy hydrothermal fluids, thus forming a relatively thick range of metasandstone.

# CONCLUSION

The following conclusions can be drawn from our study:

1) The fine-/micritic-sized calcites filling in metasandstone porosities originated from hydrothermal fluids introduced by diabase intrusion in the Funing Formation of the Gaoyou sag, while the coarse-sized calcites occurring as cements were derived from diagenetic fluids before this magmatism.
2) The flowing of hydrothermal-origin calcites was upwardly unidirectional, thus constantly forming positive drifting of strontium and oxygen isotopes. Meanwhile, this flowing was an indiscriminative breakthrough of the hydrothermal fluids in contact sandstones, regardless of permeability variations of the contact sandstones. However, the metasandstones of large pores could form a thick range of potential reservoir because of more high-energy hydrothermal fluids being accommodated.

# DATA AVAILABILITY STATEMENT

The original contributions presented in the study are included in the article/Supplementary Material, Further inquiries can be directed to the corresponding author.

## AUTHOR CONTRIBUTIONS

CL: conceptualization, methodology, writing—review and editing, and project administration. RX: formal analysis, writing—original draft. ZJ: formal analysis, investigation, visualization, and conceptualization. XZ: formal analysis, investigation, visualization, and conceptualization. KW: formal analysis, investigation, and visualization. YY: formal analysis, investigation, and visualization. JH: formal analysis, investigation, and visualization. PL: formal analysis and investigation. ZL: methodology and investigation.

## FUNDING

This project is jointly supported by the National Natural Science Foundation of China (No. 42002159) and the Foundation of State Key Laboratory of Petroleum Resources and Prospecting, China University of Petroleum, Beijing (No. PRP/open-2103).

## REFERENCES

Enrique, M., Jean-Pierre, G., and May, M. T. (1997). Diagenetic Mineralogy, Geochemistry, and Dynamics of Mesozoic Arkoses, Hartford Rift Basin, Connecticut, U. S. A. *J. Sediment. Res.* 67 (1), 212–224.

Etheridge, M. A., Wall, V. J., and Vernon, R. H. (1983). The Role of the Fluid Phase during Regional Metamorphism and Deformation. *J. Metamorph. Geol.* 1 (3), 205–226. doi:10.1111/j.1525-1314.1983.tb00272.x

Haszeldine, R. S., Samson, I. M., and Cornford, C. (1984). Quartz Diagenesis and Convective Fluid Movement: Beatrice Oilfield, UK North Sea. *Clay Min.* 19, 391–402. doi:10.1180/claymin.1984.019.3.10

Heald, M. T., and Rention, J. J. (1966). Experimental Study of Sandstone Cementation. *J. Sediment. Pet.* 36 (4), 977–991. doi:10.1306/74d715d7-2b21-11d7-8648000102c1865d

Hu, X. (2010). On the Age and Origin of the Intrusive Rocks in Gaoyou Depression of North Jiangsu Basin. *J. Stratigr.* 34 (3), 293–297. doi:10.1017/S0004972710001772

Huang, S. (1990). Cathodoluminscence and Diagenetic Alternation of Marine Carbonate Minerals. *Sediment. Geol. Teth. Geol.* 10 (4), 9–15.

Huang, S., Qing, H., Huang, P., Hu, Z., Wang, Q., Zou, M., et al. (2008). Evolution of Strontium Isotopic Composition of Seawater from Late Permian to Early Triassic Based on Study of Marine Carbonates, Zhongliang Mountain, Chongqing, China. *Sci. China Ser. D-Earth Sci.* 51 (4), 528–539. doi:10.1007/s11430-008-0034-3

Knut, B., Mo, A., and Palm, E. (1988). Modelling of Thermal Convectionin Sedimentary Basins and its Relevance to Diagenetic Reactions. *Mar. Pet. Geol.* 5, 338–350.

Korte, C., Kozur, H. W., Bruckschen, P., and Veizer, J. (2003). Strontium Isotope Evolution of Late Permian and Triassic Seawater. *Geochimica Cosmochimica Acta* 67 (1), 47–62. doi:10.1016/s0016-7037(02)01035-9

Liu, C., Gu, L., Wang, J., and Si, S. (2019). Reservoir Characteristics and Forming Controls of Intrusive-Metamorphic Reservoir Complex: A Case Study on the Diabase-Metamudstone Rocks in the Gaoyou Sag, Eastern China. *J. Petroleum Sci. Eng.* 173, 705–714. doi:10.1016/j.petrol.2018.10.063

Liu, C., Ma, J., Zhang, L., Wang, C. L., and Liu, J. (2022). Protracted Formation of Nodular Cherts in Marine Platform: New Insights from the Middle Permian Chihsian Carbonate Successions, South China. *Carbonate Evaporite* 37, 14–32. doi:10.1007/s13146-022-00757-6

Liu, C., Xie, Q., Wang, G., He, W., Song, Y., Tang, Y., et al. (2017). Rare Earth Element Characteristics of the Carboniferous Huanglong Formation Dolomites in Eastern Sichuan Basin, Southwest China: Implications for Origins of Dolomitizing and Diagenetic Fluids. *Mar. Petroleum Geol.* 81, 33–49. doi:10.1016/j.marpetgeo.2016.12.030

Liu, C., Xie, Q., Wang, G. W., Cui, Y., and Zhang, C. J. (2015). The Influence of Igneous Intrusion to Detrital Reservoir: Advances and Outlook. *Adv. Earth Sci.* 30 (6), 654–667. doi:10.11867/j.issn.1001-8166.2015.06.0654

Liu, C., Xie, Q., Wang, G., Zhang, C., Wang, L., and Qi, K. (2016). Reservoir Properties and Controlling Factors of Contact Metamorphic Zones of the Diabase in the Northern Slope of the Gaoyou Sag, Subei Basin, Eastern China. *J. Nat. Gas Sci. Eng.* 35, 392–411. doi:10.1016/j.jngse.2016.08.070

Machel, H. G., and Burton, E. A. (1994). Golden Grove Dolomite, Barbados: Origin from Modified Seawater. *J. Sediment. Res. Sect. A* 64 (4), 741–751. doi:10.1306/d4267eab-2b26-11d7-8648000102c1865d

Machel, H. G. (2004). "Concepts and Models of Dolomitization: a Critical Reappraisal," in *The Geometry and Petro-Genesis of Dolomite Hydrocarbon Reservoirs*. Editors C. J. R. Braithwaite, G. Rizzi, and G. Drake (London: Geological Society. Special Publication), 235, 7–63. doi:10.1144/gsl.sp.2004.235.01.02

Mao, F. (2000). Determination of the Forming Time of Diabase in the Northern Slope of Gaoyou Sag and its Relationship with Oil and Gas. *Pet. Explor. Dev.* 27, 19–20.

McArthur, J. M., Howarth, R. J., and Bailey, T. R. (2001). Strontium Isotope Stratigraphy: LOWESS Version 3: Best Fit to the Marine Sr-Isotope Curve for 0-509 Ma and Accompanying Look-up Table for Deriving Numerical Age. *J. Geol.* 109, 155–170. doi:10.1086/319243

Rateau, R., Schofield, N., and Smith, M. (2013). The Potential Role of Igneous Intrusions on Hydrocarbon Migration, West of Shetland. *Pet. Geosci.* 19 (3), 259–272. doi:10.1144/petgeo2012-035

Robert, J. R., Tamer, K., and James, L. P. (2005). Experimental Investigation of $CO_2$-brine-rock Interactions at Elevated Temperature and Pressure: Implications for $CO_2$ Sequestration in Deep-Saline Aquifers. *Fuel. Proc.Technol.* 86, 1581–1597. doi:10.1016/j.fuproc.2005.01.011

Ros, L. F. (1998). Heterogeneous Generation and Evolution of Diagenetic Quartzarenites in the Silurian-Devonian Furnas Formation of the Parana Basin, Southern Brazil. *Sediment. Geol.* 116, 99–128.

Therkelsen, J. (2016). Diagenesis and Reservoir Properties of Middle Jurassic Sandstones, Traill Ø, East Greenland: The Influence of Magmatism and Faulting. *Mar. Petroleum Geol.* 78, 196–221. doi:10.1016/j.marpetgeo.2016.09.017

Vahrenkamp, V. C., and Swart, P. K. (1990). New Distribution Coefficient for the Incorporation of Strontium into Dolomite and its Implications for the Formation of Ancient Dolomites. *Geol* 18 (5), 387–391. doi:10.1130/0091-7613(1990)018<0387:ndcfti>2.3.co;2

Veizer, J., Ala, D., Azmy, K., Bruckschen, K., Buhl, D., and Bruhn, F. (1999). 87Sr/86Sr, δ13C and δ18O Evolution of Phanerozoic Seawater. *Chem. Geol.* 161 (30), 59–88. doi:10.1016/s0009-2541(99)00081-9

Wang, B., Qi, D., and Wang, E. (2007). Characteristics of the Diabase and Altered Zone in BXP Area of Subei Basin and Relationship between the Diabase and the Formation of Hydrocarbon Reservoir. *J. Xi'an Pet. Inst. Nat. Sci. Ed.* 6 (6), 5–7.

Warren, J. (2000). Dolomite: Occurrence, Evolution and Economically Important Associations. *Earth Sci. Rev.* 52 (1), 1–81. doi:10.1016/s0012-8252(00)00022-2

Wood, B. J., and Walther, J. V. (1986). "Fluid Flow during Metamorphism and its Implications for Fluid-Rock Ratios," in *Fluid-Rock Interactions during Metamorphism*. Editors J. V. Walther and B. J. Wood (New York: Springer-Verlag), 89–108. doi:10.1007/978-1-4612-4896-5_4

Wu, C., Gu, L., Zhang, Z., Ren, Z., Chen, Z., and Li, W. (2006). Formation Mechanisms of Hydrocarbon Reservoirs Associated with Volcanic and Subvolcanic Intrusive Rocks: Examples in Mesozoic-Cenozoic Basins of Eastern China. *Bulletin* 90 (1), 137–147. doi:10.1306/07130505004

Yang, Q., and Chen, H. Y. (2003). Tectonic Evolution of the North Jiangsu-South Yellow Sea Basin. *Pet. Geol. Exp.* 25, 562–565.

Zhang, Y. (2000). The Lithofacies and Reservoir Model of Intrusive Rock and its Exomorphic Zones. *Pet. explor. Dev.* 27 (2), 22–26.

**Conflict of Interest:** Authors RX and XZ were employed by Changqing Oil Field Company of PetroChina. Author ZJ was employed by Research Institute of Drilling & Production Technology of Qinghai Oilfield Company. Authors PL and ZL were employed by Oil Production Plant of Huabei Oilfield Company, PetroChina.

The remaining authors declare that the research was conducted in the absence of any commercial or financial relationships that could be construed as a potential conflict of interest.

**Publisher's Note:** All claims expressed in this article are solely those of the authors and do not necessarily represent those of their affiliated organizations, or those of the publisher, the editors, and the reviewers. Any product that may be evaluated in this article, or claim that may be made by its manufacturer, is not guaranteed or endorsed by the publisher.

*Copyright © 2022 Liu, Xue, Jia, Zhao, Wang, Yang, He, Liu and Liu. This is an open-access article distributed under the terms of the Creative Commons Attribution License (CC BY). The use, distribution or reproduction in other forums is permitted, provided the original author(s) and the copyright owner(s) are credited and that the original publication in this journal is cited, in accordance with accepted academic practice. No use, distribution or reproduction is permitted which does not comply with these terms.*